Journal of Translational Medicine

RESEARCH Open Access

Chemically synthesized osteocalcin alleviates NAFLD via the AMPK-FOXO1/BCL6-CD36 pathway

Miao Zhang[1], Keting Dong[1], Qian Du[1], Jiaojiao Xu[1], Xue Bai[1], Lei Chen[1] and Jianhong Yang[1*]

Abstract

Nonalcoholic fatty liver disease (NAFLD) is a common chronic liver disease worldwide. Osteocalcin plays an important role in energy metabolism. In this study, we investigated the mechanism of action of chemically synthesized osteocalcin (csOCN) in ameliorating NAFLD. We demonstrated for the first time that csOCN attenuates lipid accumulation in the liver and hepatocytes by modulating CD36 protein expression. In addition, we found that the expression of p-AMPK, FOXO1 and BCL6 decreased and the expression of CD36 increased after OA/PA induction compared to the control group, and these effects were reversed by the addition of csOCN. In contrast, the therapeutic effect of csOCN was inhibited by the addition of AMPK inhibitors and BCL6 inhibitors. This finding suggested that csOCN regulates CD36 expression via the AMPK-FOXO1/BCL6 axis. In NAFLD mice, oral administration of csOCN also activated the AMPK pathway and reduced CD36 expression. Molecular docking revealed that osteocalcin has a docking site with CD36. Compared to oleic acid and palmitic acid, osteocalcin bound more strongly to CD36. Laser confocal microscopy results showed that osteocalcin colocalized with CD36 at the cell membrane. In conclusion, we demonstrated the regulatory role of csOCN in fatty acid uptake pathways for the first time; it regulates CD36 expression via the AMPK-FOXO1/BCL6 axis to reduce fatty acid uptake, and it affects fatty acid transport by may directly binding to CD36. There are indications that csOCN has potential as a CD36-targeted drug for the treatment of NAFLD.

Keywords Nonalcoholic fatty liver disease (NAFLD), Chemically synthesized osteocalcin (csOCN), Lipid accumulation, Molecular docking, AMPK, CD36

Introduction

Nonalcoholic fatty liver disease (NAFLD) is a spectrum of chronic liver diseases that encompasses a range of pathologies, from isolated hepatic steatosis and nonalcoholic steatohepatitis (NASH) to cirrhosis and/or hepatocellular carcinoma (HCC). NAFLD has become the most common chronic liver disease worldwide [1], and its global prevalence is approximately 25.24% (29.81% in mainland China) [2]. NAFLD seriously affects people's lives and health. Hepatocellular steatosis (or lipid accumulation), especially triglyceride (TG) accumulation, is a hallmark of NALFD and is caused by an imbalance between fatty acid sources (fatty acid uptake and de novo lipogenesis [DNL]) and fatty acid consumption (fatty acid oxidation and very low-density lipoprotein [VLDL] formation and secretion).

Osteocalcin is a small non-collagenous protein secreted by osteoblasts that is primarily deposited in the bone

*Correspondence:
Jianhong Yang
yangjh@ucas.ac.cn
[1]Medical School, University of Chinese Academy of Sciences, Beijing 101400, China

matrix. In the endoplasmic reticulum, newly synthesized osteocalcin is post-translationally modified, undergoes γ-carboxylation, acquires a greater affinity for hydroxyapatite, and is deposited in the bone matrix to participate in bone mineralization. During bone remodeling, the osteocalcin deposited in the bone matrix is decarboxylated by osteoclast acidification to carboxylated incomplete osteocalcin (including uncarboxylated osteocalcin [GluOC]), which is released and distributed throughout the body to act as an endocrine hormone. Our preliminary results suggest that GluOC alleviates hepatocyte steatosis by inhibiting the fatty acid synthesis pathway [3]. However, due to the low molecular weight of osteocalcin, its prokaryotic expression is difficult. Although the spatial structure of osteocalcin is simple, it is more convenient to construct via chemical synthesis, and it effectively controls the post-translational modification of the protein. Therefore, we chose chemical synthesis to construct osteocalcin. Chemical synthesis of a segment of the active region of osteocalcin stimulates osteoblast differentiation and extracellular machinery mineralization [4]. This finding suggested that the active region of chemically synthesized osteocalcin has osteocalcin activity. However, whether the full amino acid sequence of chemically synthesized osteocalcin has the same potency as prokaryotically expressed synthetic osteocalcin is not known.

Adenosine monophosphate-activated protein kinase (AMPK) is a heterotrimeric complex consisting of one catalytic subunit (α) and two regulatory subunits (β and γ), and it is a key sensor and regulator of cellular energy status [5]. The AMPK signaling pathway plays an important role in NAFLD. Activation of AMPK alleviates NAFLD [6–8]. CD36 is a multifunctional signaling molecule with several known ligands including long-chain FFAs, the native lipoproteins HDL, LDL and VLDL, and modified lipoproteins, including oxidized LDL (oxLDL). CD36 plays an important role in NAFLD. The overexpression of CD36 promotes the progression of NAFLD. It plays an important role in fatty acid uptake [9], DNL [10], fatty acid oxidation [11], VLDL secretion [12] and lipophagy [13]. However, whether csOCN plays a role in the development and progression of NAFLD via CD36 is not clear.

In this study, we focused on the role of csOCN with CD36. For the first time, we found that csOCN alleviated lipid accumulation in hepatocytes by inhibiting CD36 expression via the AMPK-FOXO1/BCL6 pathway. In addition, we found that csOCN might bind to CD36 on the cell membrane surface to block its binding to fatty acids, which prevented fatty acid uptake. These results provide a new ideas for the prevention and treatment of NAFLD.

Materials and methods

Cells and cell culture

The mouse normal hepatocyte cell line NCTC 1469 was purchased from Procell Life Science & Technology (Wuhan, China) and maintained according to the manufacturer's instructions. For treatment, the hepatocyte steatosis model induced with OA/PA (0.5/0.25 mM) was treated with or without csOCN (9 ng/mL) for 24 h. In the inhibition of AMPK activation assay, the cells were first pretreated with 10 μM dorsomorphin (Compound C, CpdC; HY-13418 A, MedChemExpress, Shanghai, China) (an AMPK inhibitor) or DMSO as a vehicle control for 1 h followed by treatment with csOCN or PBS as a vehicle control in fresh induction medium for another 24 h. In an experiment to inhibit the activity of BCL6, the cells were pretreated with 50 μM CID5721353 (compound 79−6, 79−6; HY-100502, MedChemExpress, Shanghai, China) (a BCL6 inhibitor) or DMSO as a vehicle control for 24 h prior to csOCN treatment for an additional 24 h in media containing OA/PA. We constructed a recombinant mouse GST-osteocalcin fusion protein and used DE3 (TransGen Biotech, China) to express the reconstructed GluOC. csOCN was purchased from Sangon Biotech, and it is a chemical synthesis of mouse osteocalcin (46 aa) with a C19-C25 disulfide bond modification.

Establishment of NAFLD model mice

Six-week-old male C57BL/6J wild-type mice (weighing between 20 and 21 g) were obtained from Beijing Vital River Laboratory Animal Technology Co., Ltd. The mice were randomly divided into four groups, one on a normal control diet (NCD; 11.8% fat, 65.1% carbohydrates, 23.0% protein; BEIJING KEAO XIELI FEED Co., Ltd.; Beijing, China), and the other three on a high-fat diet (HFD; 40% fat, 40% carbohydrate, 23% protein; Dyets; Wuxi, China). The HFD mice were treated with vehicle (PBS), low-dose csOCN (OC-L; 3 ng/g body weight/day) or high-dose csOCN (OC-H; 10 ng/g body weight/day) via oral gavage for 4 weeks after 11 weeks on a HFD. Mice were housed in barrier facilities and maintained on a 12 h/12 h light/dark cycle. The feeding conditions included adequate food and water and a comfortable temperature of 24±1 °C. The animal experimental protocols used in this study were approved by the University of Chinese Academy of Sciences Animal Care and Use Committee.

CD36 knockdown

SiRNAs targeting mouse CD36 (siRNA-1136, sense: GCCAUAAUUGAGUCCUAUAAATT and antisense: UUUAUAGGACUCAAUUAUGGCTT; siRNA-1300, sense: CGGAUCUGAAAUCGACCUUAATT and antisense: UUAAGGUCGAUUUCAGAUCCGTT; siRNA-1624, sense: GCAGGUCAACAUAUUGGUCAATT and antisense: UUGACCAAUAUGUUGACCUGCTT) and nontargeting

control siRNA were purchased from Sangon Biotech (Shanghai, China). The siRNAs were transfected into NCTC 1469 cells using Hieff Trans Liposomal Transfection Reagent (40802ES03, Yeasen, Shanghai, China) according to the manufacturer's recommendations.

Lentiviral vector construction and transfection

CD36-overexpressing cells were generated using lentivirus-based vectors from GeneChem (Shanghai, China). After transfection, the cells were selected at 6 μg/mL Puromycin (HY-K1057, MedChemExpress, Shanghai, China) for 72 h. The efficacy of lentivirus transfection was validated by the fluorescence efficiency of GFP, qPCR or Western blotting.

Cell staining

After induction and treatment, the cells were fixed and permeabilized as needed. The cells were stained with Oil Red O (O8010; Solarbio, Beijing, China) working solution for 60 min, Nile Red solution (HY-D0718; MedChemExpress, Shanghai, China) for 30 min, or BODIPY 493/503 solution (GC42959; GLPBIO, Shanghai, China) for 30 min at room temperature. The sections were rinsed with distilled water and coverslipped. The sections were imaged with a light microscope (Leica Microsystems, Wetzlar, Germany).

Fatty acid uptake assay

The fatty acid uptake capacity of NCTC 1469 cells was determined using the Screen Quest™ Fluorimetric Fatty Acid Uptake Assay Kit (36385, AAT Bioquest, USA) according to the manufacturer's instructions. Briefly, NCTC 1469 cells were seeded in 96-well plates at 5.0×10^3 cells per well. After 12 h, the cells were treated with or without 9 ng/mL csOCN for an additional 24 h. The medium was replaced with serum-free medium for 1 h, followed by the addition of 100 μL of fluorescent fatty acid substrate for an additional 1 h. The cellular fluorescence intensity was monitored using BioTek Synergy H1 (Agilent, USA).

Evaluation of hepatic lipid accumulation

For in vitro experiments, triglyceride analysis of NAFLD cell models was performed using a triglyceride reagent kit (E1013; Applygen, Beijing, China). Mice were sacrificed after 4 weeks of csOCN administration. Blood glucose, LDL-C, TC and TG were determined in blood and liver tissues using a blood glucose content assay kit (Solarbio, Beijing, China), a low-density lipoprotein cholesterol (LDL-C) content assay kit (BC5335; Solarbio, Beijing, China), a total cholesterol assay kit (A111-1-1; Nanjing Jiancheng Bioengineering Institute, Nanjing, China) and a triglyceride assay kit (A110-1-1; Nanjing Jiancheng Bioengineering Institute, Nanjing, China), respectively, and liver sections were stained with Oil Red O and hematoxylin and eosin (G1120; H&E; Solarbio, Beijing, China). All of these procedures were performed according to the manufacturer's protocol.

Quantitative real-time PCR

Total RNA was isolated using an RNA purification kit (BS259A, Biosharp, Anhui, China) according to the manufacturer's instructions. Reverse transcription reactions for cDNA were performed using the Hifair III 1st Strand cDNA Synthesis SuperMix for qPCR (11141ES60, Yeasen, Shanghai, China) according to the manufacturer's protocol. PCR amplification was performed using TransStart Top Green qPCR SuperMix (+Dye II) (AQ132-24; TransGen Biotech, Beijing, China). The primers used are listed in Table 1. The results were normalized to the expression of β-actin and calculated using the $2^{-\Delta\Delta Ct}$ method.

Western blot analysis

RIPA lysis buffer (R0010; Solarbio, Beijing, China) was used to extract total protein according to the manufacturer's protocol. Total protein lysates were centrifuged at 12,000 g for 15 min at 4 °C. We then collected the supernatants for protein concentration determination using a BCA detection kit (B5000; Lablead Biotech, Beijing, China). For electrophoresis, 40 μg of total protein was added to each lane. Primary antibodies were incubated overnight at 4 °C. Primary antibodies against anti-AMPK alpha 1 (phospho T183) + AMPK alpha 2 (phospho T172)

Table 1 Primers for RT-qPCR

Gene symbol	NCBI Reference Sequence	Forward Primer (5′→3′)	Reverse Primer (5′→3′)
FOXO1	NM_019739.3	CTACGAGTGGATGGTGAAGAGC	CCAGTTCCTTCATTCTGCACTCG
BCL6	NM_009744.5	CCGGCACGCTAGTGATGTT	TGTCTTATGGGCTCTAAACTGCT
CD36	NM_007643.4	ATGGGCTGTGATCGGAACTG	TTTGCCACGTCATCTGGGTTT
FABP1	NM_017399.5	AGTCGTCAAGCTGGAAGGTGACAA	GACAATGTCGCCCAATGTCATGGT
FATP2	NM_011978.2	ACACACCGCAGAAACCAAATGACC	TGCCTTCAGTGGATGCGTAGAACT
FATP5	NM_009512.2	TGTAACGTCCCTGAGCAACCAGAA	ATTCCCAGATCCGAATGGGACCAA
β-actin	NM_007393.5	GATCTGGCACCACACCTTCT	GGGGTGTTGAAGGTCTCAAA

(ab133448) were purchased from Abcam (Cambridge, MA, USA). Primary antibodies against AMPKα (D5A2) rabbit mAb (5831) was purchased from Cell Signaling Technology (Danvers, MA, USA). Primary antibodies against FATP2 polyclonal antibody (14048-1-AP), TFEB polyclonal antibody (13372-1-AP), β-actin recombinant antibody (81115-1-RR) and α-tubulin polyclonal antibody (11224-1-AP) were purchased from Proteintech Group (Chicago, IL, USA). Primary antibodies against CD36 (bs-8873R) and anti-FOXO1 (bs-23175R) were purchased from Bioss (Beijing, China). Primary antibodies against anti-Bcl-6 rabbit pAb (WL03134) were purchased from Wanleibio (Wuhan, China). Secondary goat anti-rabbit IgG (H+L)-HRP (S0101) and goat anti-mouse IgG (H+L)-HRP (S0100) were purchased from Lablead Biotech (Beijing, China). The protein bands were visualized using an enhanced chemiluminescence (ECL) kit (1705060; Bio-Rad, Hercules, CA, USA). Relative changes in protein expression were detected using β-actin as an internal reference. ImageJ software (version 1.5.3e; National Institutes of Health, Bethesda, MA, USA) was used for protein quantification.

Statistical analysis

All experiments were performed with three or more independent replicates.The data are presented as the means±SD. Statistical analysis was performed using GraphPad Prism version 9.0 (GraphPad Software, Inc., La Jolla, CA, USA). Statistical differences between two groups were determined using two-tailed Student's t tests. $P<0.05$ indicated a statistically significant difference.

Results

csOCN inhibits lipid accumulation in OA/PA-induced NCTC 1469 cells

To investigate the effect of csOCN on OA/PA-induced lipid accumulation in NCTC 1469 cells, we used Oil Red O, Nile Red, BODIPY 493/503, and TG analyses to detect lipids in the cells. The amino acid sequence (one letter amino acid codes) of mouse osteocalcin is shown in Fig. 1A. As shown in Fig. 1B, the TG content was significantly increased in the OA/PA-induced group compared to the control group. However, after the csOCN and GluOC treatment, the TG content in the cells decreased and there was no significant difference between the csOCN- and GluOC-treated groups. Subsequent Oil Red O staining, Nile Red staining and BODIPY 493/503 staining demonstrated this phenomenon (Fig. 1C-F). These results indicated that csOCN and GluOC alleviated OA/PA-induced lipid accumulation in hepatocytes.

csOCN decreases the expression of fatty acid uptake-related genes and proteins

Fatty acid uptake pathways play important roles in hepatocellular steatosis. We found that fatty acid uptake was decreased in NCTC 1469 cells after csOCN pretreatment compared to normal cells (Fig. 2A). Genes associated with fatty acid uptake were subsequently analyzed (Fig. 2B-F). The results showed that csOCN treatment suppressed the OA/PA-induced high expression of CD36, FATP1, FATP2, FATP5, and GPR40 mRNA. We also examined the mRNA expression of BCL6, which correlates with CD36 transcription. The mRNA expression of BCL6 decreased after OA/PA induction, and the transcript level of BCL6 increased after csOCN treatment (Fig. 2G). The protein levels of CD36 and FATP2 were consistent with the changes in mRNA expression (Fig. 2H-I). These findings suggested that csOCN inhibited the expression of genes and proteins related to fatty acid uptake.

csOCN attenuates lipid accumulation in NCTC 1469 cells via CD36

The mRNA and protein expression of CD36 was significantly increased in the OA/PA group compared to the control group, but the increase in CD36 expression was reversed after csOCN treatment (Fig. 2B, H). CD36 plays an important role in fatty acid uptake. This finding suggests that CD36 mediated csOCN inhibition of the fatty acid uptake pathway.

To investigate whether csOCN alleviated hepatocyte lipid accumulation by reducing CD36, we compared the effects of csOCN treatment and CD36 knockdown on hepatocyte lipid accumulation. First, we used siRNA to knockdown CD36. As shown in Fig. 3A, in NCTC 1469 cells transfected with siRNA-CD36-1136, siRNA-CD36-1300, or siRNA-CD36-1624, the expression of CD36 was significantly suppressed, and the knockdown efficiency was greater in the siRNA-CD36-1300 group. Therefore, siRNA-CD36-1300 (hereinafter abbreviated as si-CD36) was selected for use in subsequent experiments. The expression level of CD36 decreased after CD36 was knocked down (Fig. 3B). As shown in Fig. 3C-F, Nile Red staining, BODIP 493/503 staining, and triglyceride assays showed that si-CD36 and csOCN reduced the OA/PA-induced increase in intracellular lipid accumulation, and there was no significant difference between the effects of si-CD36 and csOCN on reducing intracellular lipid accumulation. This finding suggested that csOCN alleviated OA/PA-induced hepatocyte steatosis by inhibiting CD36 expression.

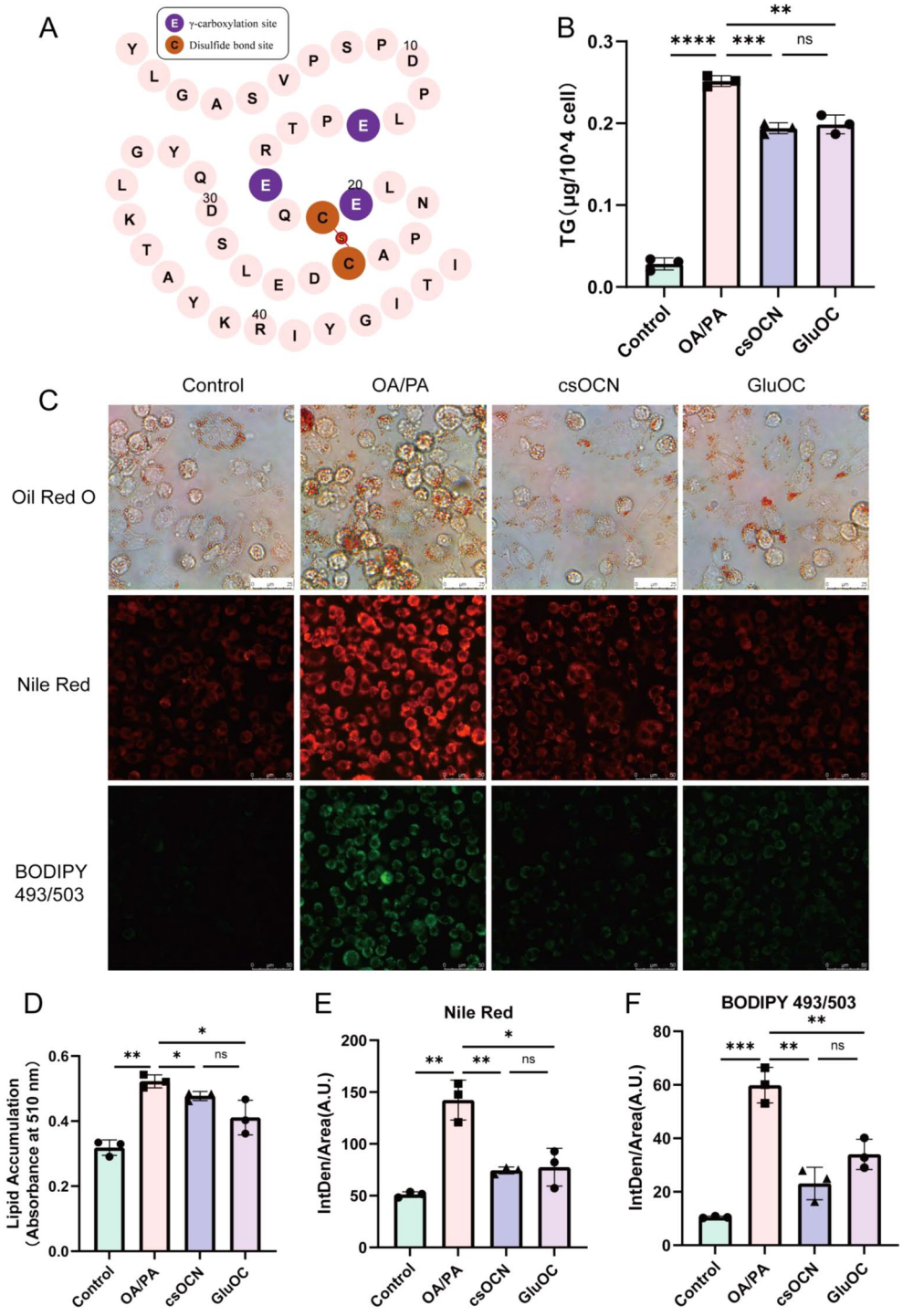

Fig. 1 csOCN ameliorated OA/PA-induced lipid accumulation in hepatocytes. (**A**) Amino acid sequence of mouse osteocalcin. (**B**) TG accumulation in NCTC 1469 cells was assessed according to the instructions of the Triglyceride Content Assay Kit (BC0625, Solarbio). (**C**) Representative photomicrographs of Oil Red O staining, Nile Red staining and BODIPY 493/503 staining (200×). (**D**) Absorbance analysis of Oil Red O dye after elution with isopropanol. (**E**) Mean fluorescence intensity of Nile Red staining in Fig. 1C. (**F**) Mean fluorescence intensity of BODIPY 493/503 staining in Fig. 1C. The data are presented as the means ± SD of three independent experiments. * $p < 0.05$, ** $p < 0.01$, *** $p < 0.001$, and **** $p < 0.0001$. OA/PA, oleic acid, and palmitic acid; csOCN, oleic acid, and palmitic acid + chemically synthesized osteocalcin; GluOC, OA/PA + uncarboxylated osteocalcin

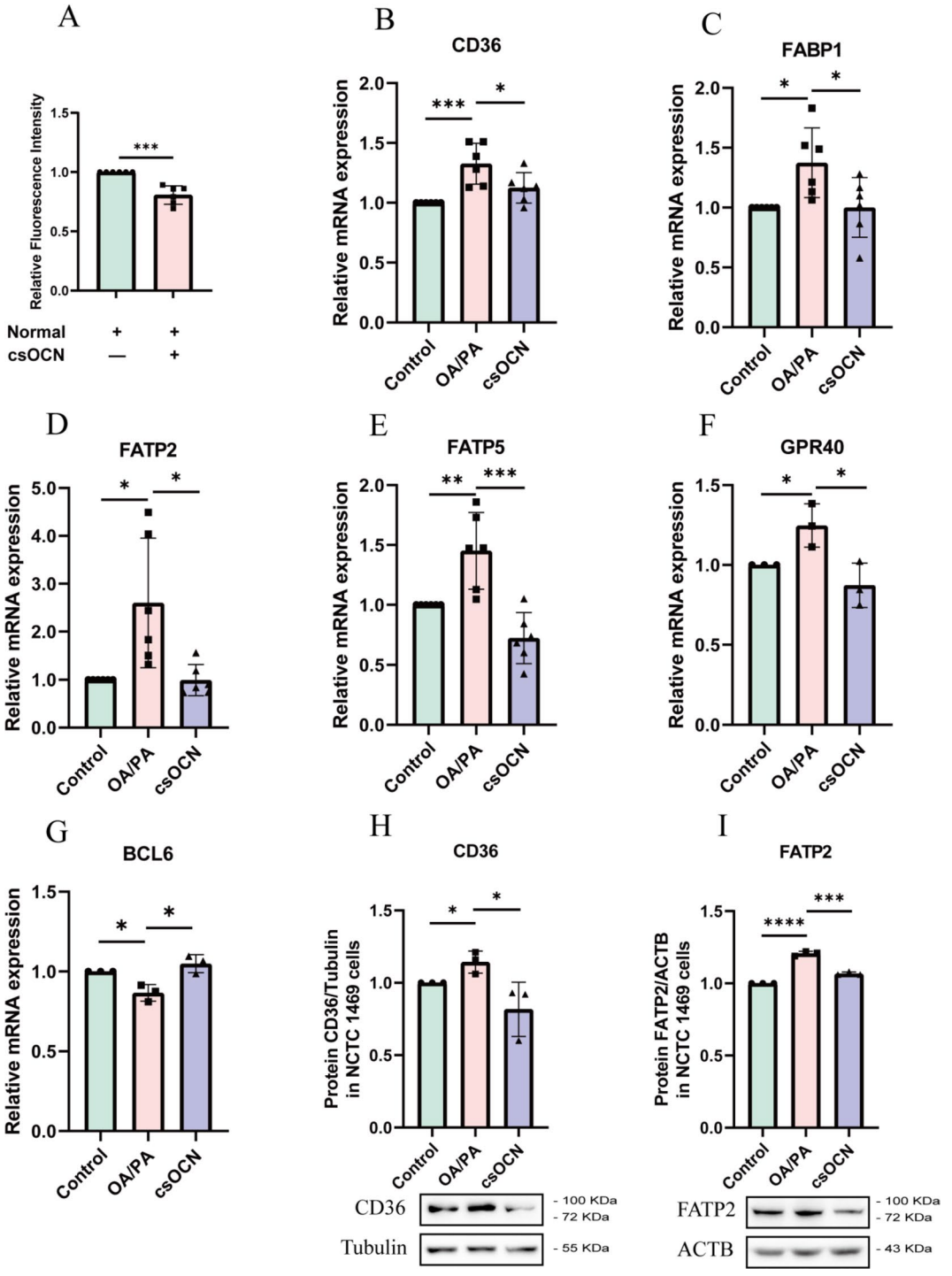

Fig. 2 csOCN reduced OA/PA-induced increases in the expression of genes associated with fatty acid uptake in hepatocytes. (**A**) csOCN alleviates fatty acid uptake by hepatocytes. (**B-F**) csOCN decreased the OA/PA-induced increase in the mRNA expression of CD36, FABP1, FATP2, FATP5 and GPR40 in NCTC 1469 cells. (**G**) csOCN enhanced the OA/PA-induced decrease in BCL6 mRNA expression. (**H-I**) csOCN reduced the OA/PA-induced increase in the protein expression of CD36 and FATP2 in NCTC 1469 cells. The data are presented as the means ± SD of more than three independent experiments. * $p < 0.05$, ** $p < 0.01$, *** $p < 0.001$, **** $p < 0.0001$

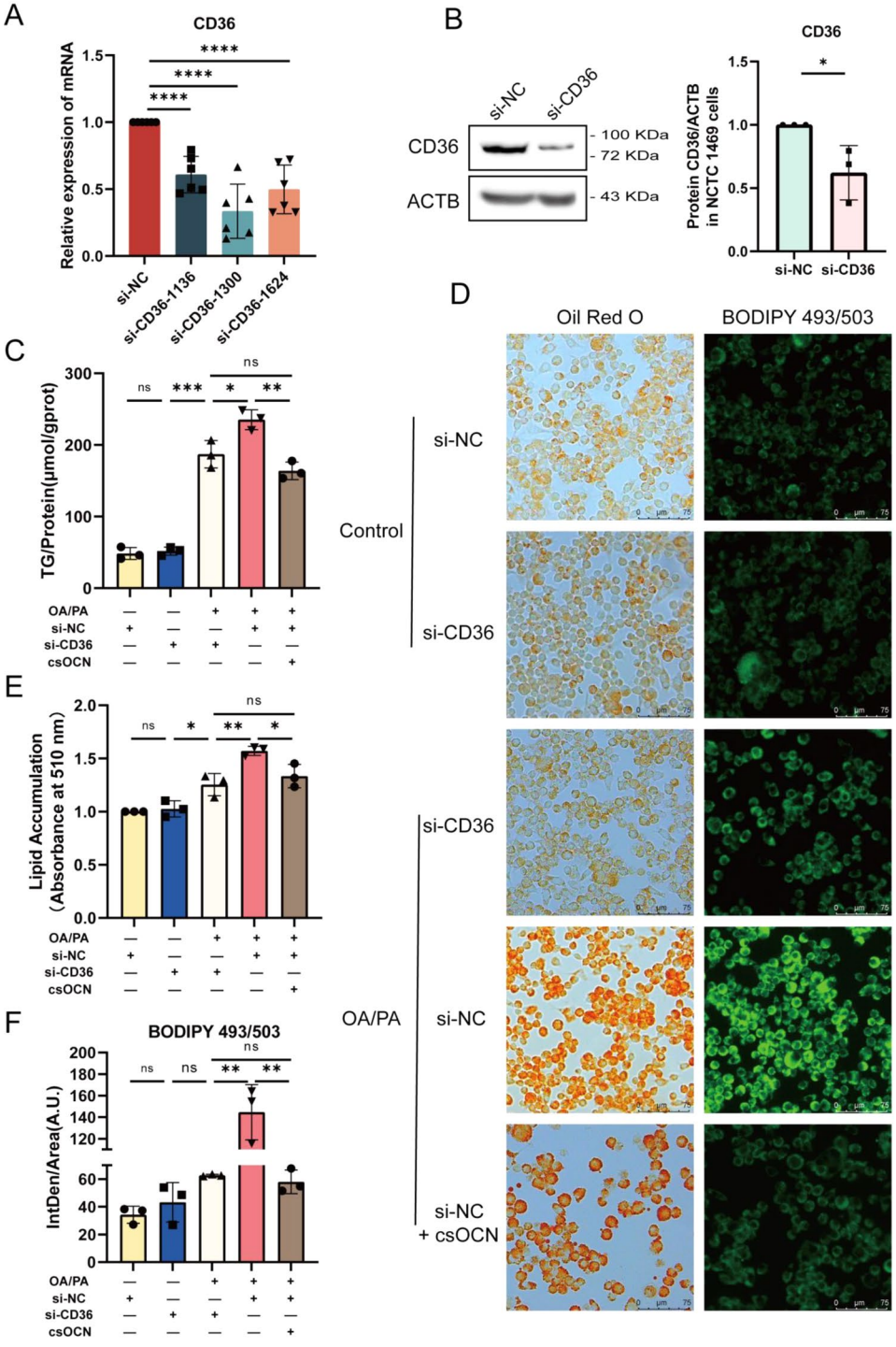

Fig. 3 csOCN attenuates lipid accumulation in NCTC 1469 cells via CD36. (**A**) siRNA-CD36-1136, siRNA-CD36-1300, and siRNA-CD36-1624 all significantly suppressed CD36 mRNA expression. The data are presented as the means ± SD of six independent experiments. **** $p < 0.0001$ versus the si-NC group. (**B**) Protein expression of CD36 after transfection. (**C**) csOCN treatment and CD36 knockdown reduced TG levels in the NCTC 1469 cells exposed to OA/PA. (**D**) Oil red O staining and BODIPY 493/503 staining showed that csOCN treatment and CD36 knockdown reduced lipid accumulation in NCTC 1469 cells exposed to OA/PA (200×). (**E**) Absorbance analysis of the Oil red O dye after isopropanol elution. (**F**) The mean fluorescence intensity of BODIPY 493/503 staining in Fig. 3C. The data are presented as the means ± SD of three independent experiments. * $p < 0.05$, ** $p < 0.01$, *** $p < 0.001$. Control + si-NC, Control + siRNA-negative control; Control + si-CD36, Control + siRNA-CD36; OA/PA + si-CD36, oleic acid and palmitic acid + siRNA-CD36; OA/PA + si-NC, oleic acid and palmitic acid + siRNA-negative control; OA/PA + si-NC + csOCN, oleic acid and palmitic acid + siRNA-negative control + chemically synthesized osteocalcin

csOCN alleviates lipid accumulation induced by the overexpression of CD36

To further validate the roles of csOCN and CD36, the following experiments were designed with and without CD36 overexpression. First, we established a CD36-overexpression cell line (OE-CD36) using lentivirus-infected NCTC 1469 cells and measured the expression of CD36 mRNA and protein. As shown in Fig. 4A-B, the expression of CD36 was increased in the OE-CD36 group compared to the CON136 group (Lenti-control). We then examined the effect of CD36 and csOCN on fatty acid uptake by hepatocytes. As shown in Fig. 4C, fatty acid uptake decreased in the CON136 group after pretreatment with csOCN. In CD36-overexpressing cells, fatty acid uptake also decreased after pretreatment with csOCN, but it was still higher than the CON136 group. This finding suggested that csOCN attenuated the enhanced fatty acid uptake induced by CD36 overexpression. We then investigated the effect of csOCN on lipid accumulation in hepatocytes in the presence or absence of CD36 overexpression. BODIPY 493/503 staining, Oil Red O staining, and triglyceride assays revealed that OE-CD36 exacerbated OA/PA-induced intracellular lipid accumulation compared to the CON136 group, but the addition of csOCN alleviated intracellular lipid accumulation in the OE-CD36 group (Fig. 4D-H). These results indicated that csOCN alleviated the lipid accumulation induced by CD36 overexpression. In conclusion, csOCN reduced lipid accumulation in hepatocytes by alleviating the enhanced fatty acid uptake caused by CD36 overexpression.

Activation of AMPK by csOCN inhibits CD36 expression via FOXO1

Our previous results showed that GluOC promoted AMPK phosphorylation. However, csOCN also affected the expression of CD36 in the present study. To investigate whether AMPK mediated csOCN regulation of CD36, we used the AMPK inhibitor CpdC to inhibit AMPK activation. First, we examined the effect of different concentrations of CpdC on AMPK phosphorylation in hepatocytes (Fig. 5A) and selected 10 μM as the working concentration. We then analyzed the role of CpdC in the therapeutic effect of csOCN by detecting the lipid metabolism-related proteins AMPK, FOXO1 and CD36 in hepatocytes (Fig. 5B-D). We found that csOCN activated AMPK and promoted FOXO1 expression while inhibiting the expression of CD36, and CpdC reversed the effect of csOCN. We also investigated the effects of csOCN and CpdC treatment on the nuclear localization of FOXO1 (Fig. 5E). We found that the intensity of FOXO1 fluorescence in the nucleus decreased after OA/PA induction compared to the control group, but the expression of FOXO1 fluorescence in the nucleus increased after csOCN treatment. The effect of csOCN was reversed after CpdC treatment. These results suggest that activation of the AMPK pathway by csOCN promotes FOXO1 expression and nuclear localization and inhibits CD36 expression.

Activation of AMPK by csOCN inhibits CD36 expression via BCL6

The expression of BCL6 mRNA was significantly reduced in the OA/PA group compared to the control group, but this difference was reversed after csOCN treatment (Fig. 2G). The effect of csOCN on BCL6 expression was investigated using the AMPK inhibitor CpdC. As shown in Fig. 6A, csOCN reversed the OA/PA-induced decrease in BCL6 expression, and this effect was attenuated by the addition of CpdC. We used the BCL6 transcriptional activity inhibitor 79−6 to block the effects of BCL6. We first examined the effects of different concentrations of BCL6 inhibitors on cell proliferation (Fig. 6B), BCL6 mRNA expression (Fig. 6C), CD36 mRNA expression (Fig. 6D), and GPR40 mRNA expression (Fig. 6E). Based on these results, we selected 50 μM 79−6 as the working concentration. We then investigated the effect of 79−6 on the therapeutic efficacy of csOCN. The results showed that the OA/PA-induced decrease in BCL6 expression was reversed by the addition of csOCN, but the protein expression of BCL6 was not affected by the addition of 79−6 (Fig. 6F), which was consistent with the effect of 79−6. As shown in Fig. 6G, csOCN treatment attenuated the OA/PA-induced increase in CD36 expression, and the addition of a 79−6 inhibitor reversed the therapeutic effect of csOCN. In conclusion, the activation of AMPK by csOCN promoted BCL6 expression and inhibited CD36 transcription.

Molecular docking

In the present study, we also performed molecular docking analyses to investigate the possible interactions of osteocalcin and fatty acids with CD36. Figure 7A shows the binding position of osteocalcin with CD36. Hydrogen bonds cannot be formed due to the lack of an amino hydrogen on the proline residue. Therefore, osteocalcin only forms hydrogen bonds with CD36 at Asn-31, Tyr-291, and Glu-282. In addition, osteocalcin forms a salt bridge with CD36 at Glu-282. These forces help stabilize the binding position of CD36 at the ligand binding site (Table 2). Figure 7B shows the interaction binding site of oleic acid with CD36. The three-dimensional interaction diagram shows the hydrogen bond formed by oleic acid at ASN-118 on the CD36 molecule and the salt bridges at Arg-63, Arg-96 and Ala-251, Phe-266, Ile-271, Ile-275, Leu-295, Leu-371, Lys-385, and Leu-387 on the hydrophobic interactions of the CD36 protein (Table 3), and these interaction forces stabilize the binding of oleic acid

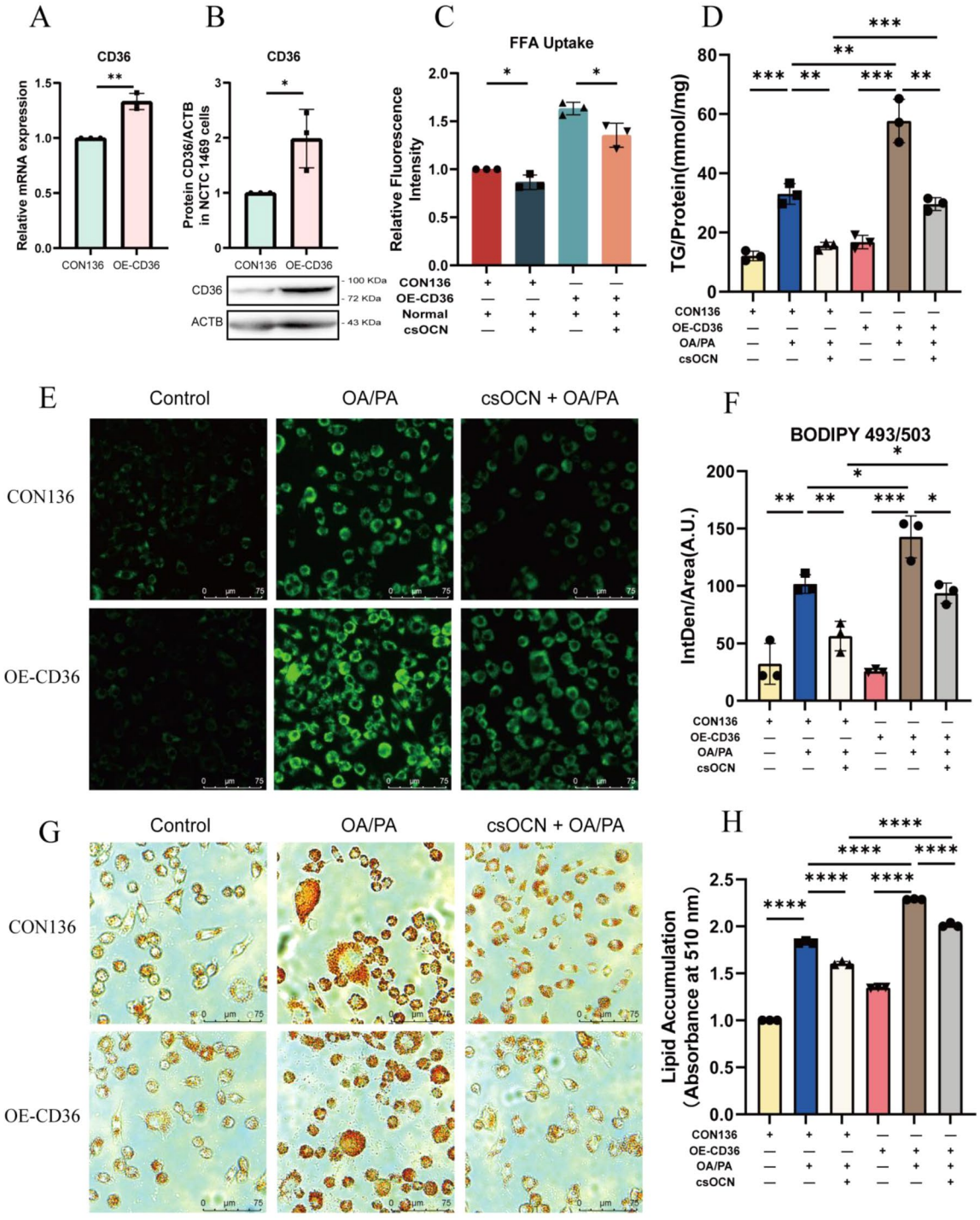

Fig. 4 csOCN alleviates lipid accumulation caused by CD36 overexpression. (**A**) CD36 mRNA levels after lentiviral infection. (**B**) Protein expression of CD36 after lentiviral infection. (**C**) csOCN attenuates the increase in fatty acid uptake caused by CD36 overexpression. (**D**) CD36 overexpression increased OA/PA-induced TG levels in NCTC 1469 cells, but csOCN attenuated the increase in TG content caused by CD36 overexpression. (**E**) BODIPY 493/503 staining (200×). (**F**) The mean fluorescence intensity of BODIPY 493/503 staining in Fig. 4E. (**G**) Oil red O staining (200×). (**H**) Analysis of the absorbance Oil Red O-stained cells after elution with isopropanol. The data are presented as the means ± SD of three independent experiments. * $p < 0.05$, ** $p < 0.01$, *** $p < 0.001$, **** $p < 0.0001$

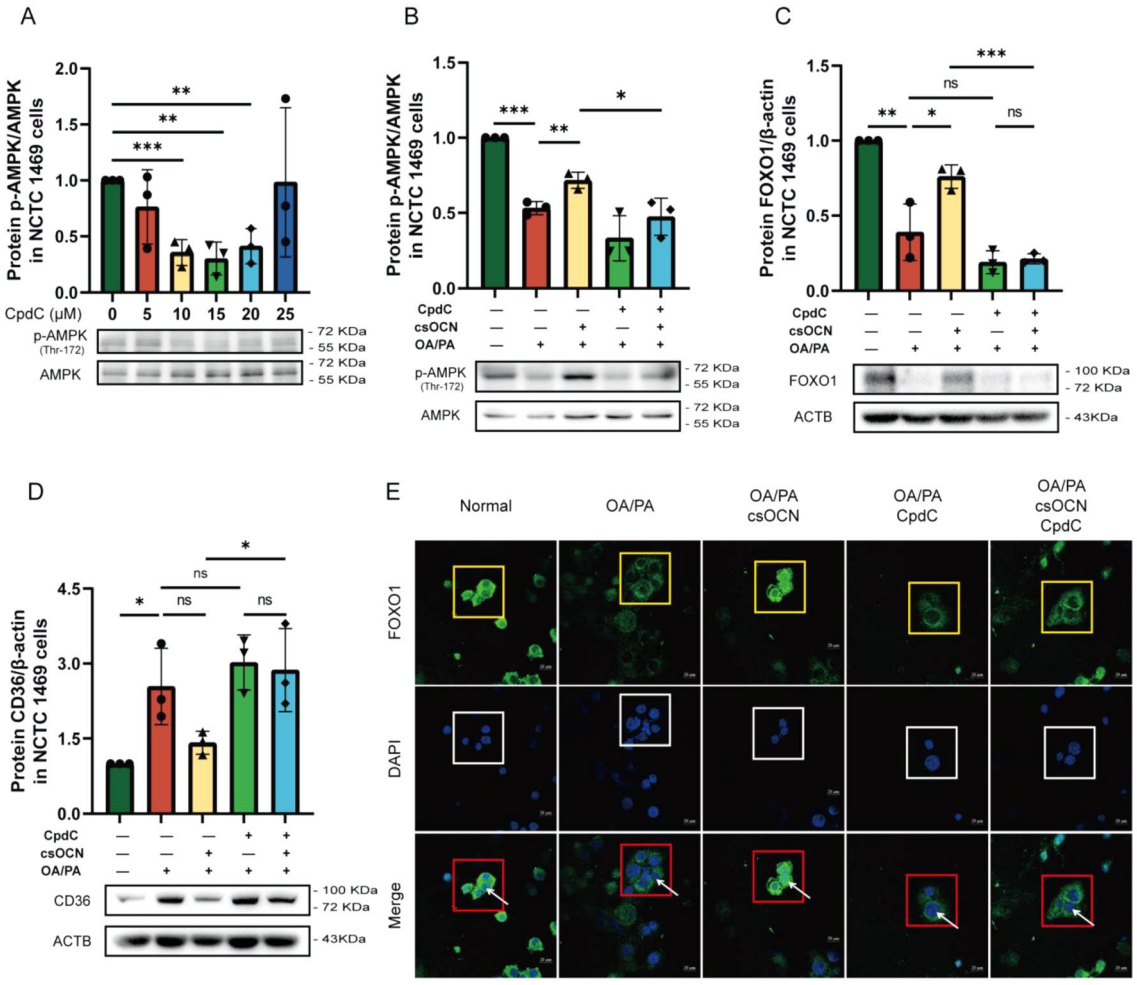

Fig. 5 csOCN activates AMPK and inhibits CD36 expression via FOXO1. (**A**) Effects of different concentrations of CpdC on AMPK phosphorylation in NCTC 1469 cells. (**B**) csOCN increased the OA/PA-induced decrease in AMPK phosphorylation, and CpdC reversed this effect of csOCN. (**C**) csOCN increased the OA/PA-induced decrease in FOXO1 expression, and CpdC reversed this effect of csOCN. (**D**) csOCN inhibited the OA/PA-induced increase in CD36 expression, and CpdC reversed this effect of csOCN. (**E**) Nuclear localization of total FOXO1. csOCN increased the OA/PA-induced decrease in FOXO1 nuclear localization (white arrows), and CpdC reversed this effect of csOCN. The data are presented as the means ± SD of three independent experiments. * $p < 0.05$, ** $p < 0.01$, *** $p < 0.001$

to CD36. Figure 7C shows the binding posture of palmitic acid and CD36 and its three-dimensional interactions with hydrogen bonds formed at Gly-199 and salt bridges at Lys-337; and its hydrophobic interactions at Leu-140, Ala-144, Val-198, Val-200, Lys-334, Lys-337, Val-339, and Val-389 (Table 3). These interaction forces are the basis for maintaining the palmitic acid-CD36 complex formation. A negative binding affinity indicates the possibility of binding, and typically, smaller values indicate a higher probability of binding. In this analysis, osteocalcin, oleic acid and palmitic acid had binding affinities of -11.0 kcal/mol, -6.6 kcal/mol and -5.7 kcal/mol, respectively, for CD36 (Table 4), which suggests that osteocalcin binds more strongly to CD36 than oleic acid and palmitic acid.

Osteocalcin may colocalized with CD36

We determined whether there was an intermolecular interaction between OCN and CD36. Lentiviral infection of NCTC 1469 cells was used to establish a GFP-labeled CD36-overexpressing cell line, as shown in Fig. 8A, which shows the GFP fluorescence intensity of the CD36-overexpressing cell line. We treated the cells with rhodamine B-labeled OCN and analyzed the colocalization of OCN and CD36 using laser confocal microscopy. As shown in Fig. 8B, there was an overlap between the red fluorescent signal and the green fluorescent signal in the cell. As shown in Fig. 8C, we knocked down CD36 in NCTC 1469 cells using siRNA then treated the cells with rhodamine B-labeled OCN. The results showed a weakened red fluorescence signal after knockdown of CD36 compared to the control. These results suggest that OCN may bind to CD36.

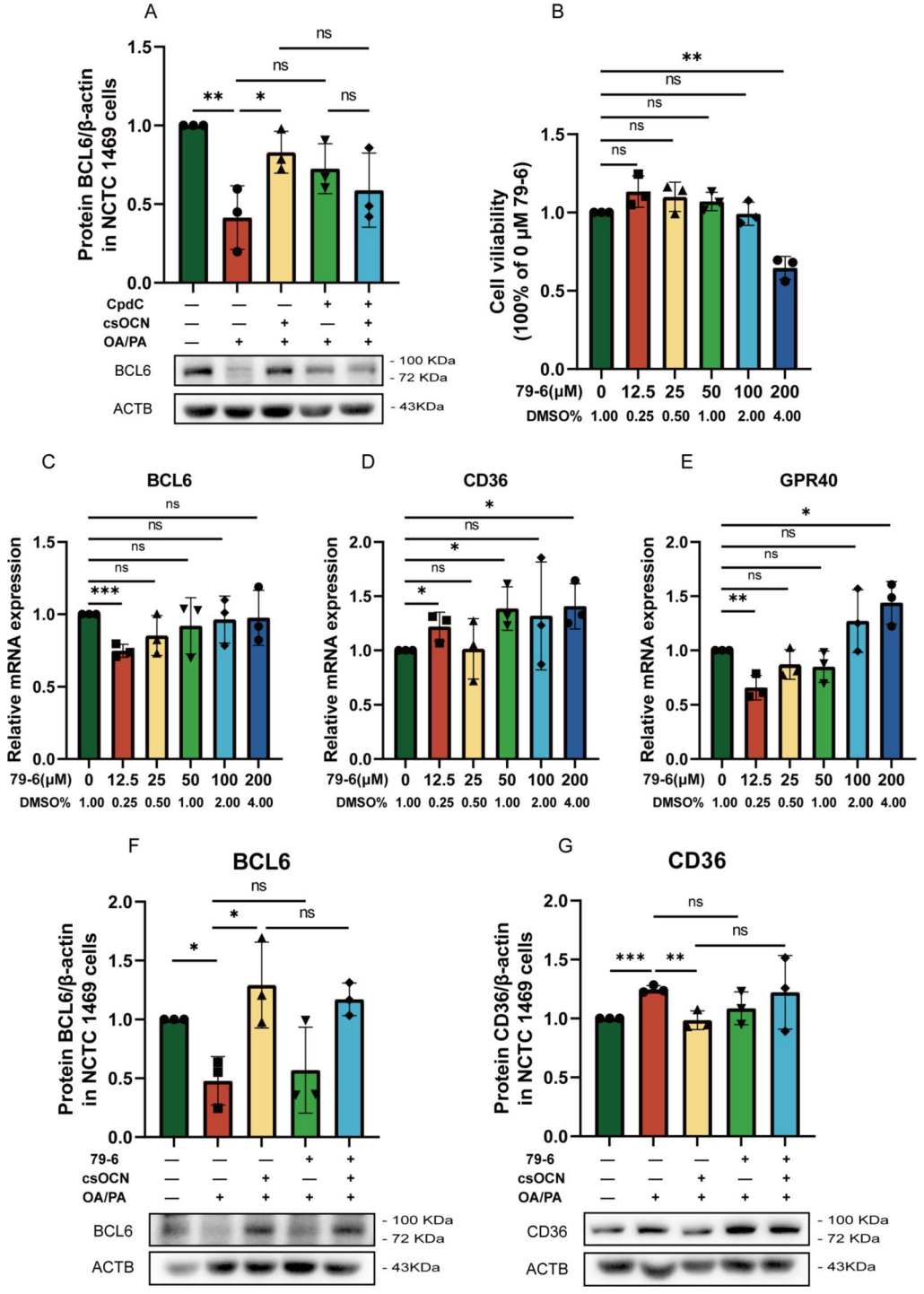

Fig. 6 csOCN activates AMPK and inhibits CD36 expression via BCL6. (**A**) csOCN increased the OA/PA-induced decrease in the expression of BCL6. (**B**) Cytotoxicity of different concentrations of 79 – 6 on hepatocytes. (**C**) Effects of different concentrations of 79 – 6 on BCL6 mRNA expression. (**D**) Effects of different concentrations of 79 – 6 on CD36 mRNA expression. (**E**) Effects of different concentrations of 79 – 6 on GPR40 mRNA expression. (**F**) Treatment with 50 μM 79 – 6 did not affect the effect of csOCN on BCL6 protein expression. (**G**) Treatment with 50 μM 79 – 6 reversed the inhibitory effect of csOCN on the CD36 protein. The data are presented as the means ± SD of three independent experiments. * $p < 0.05$, ** $p < 0.01$, *** $p < 0.001$

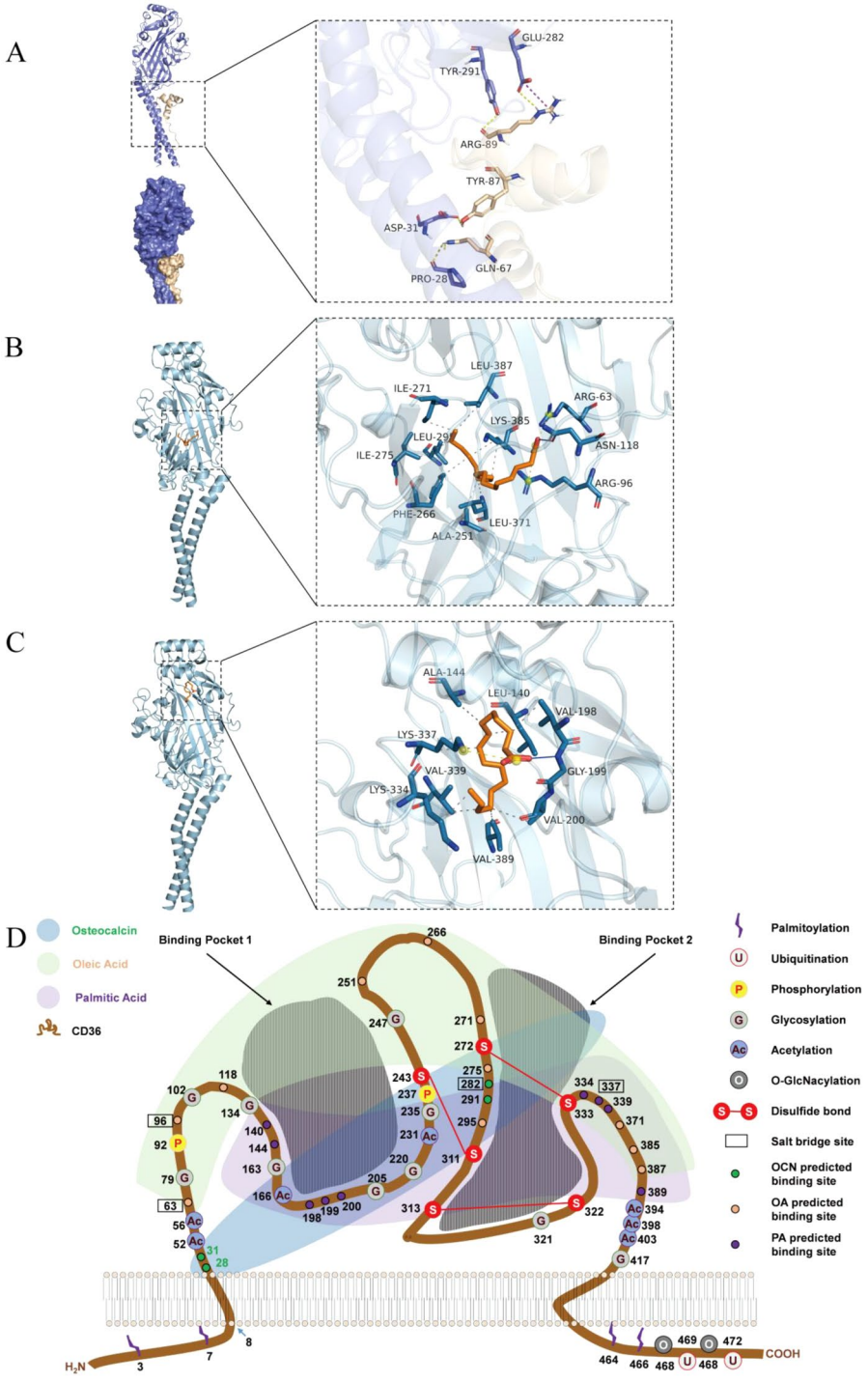

Fig. 7 Computer simulation to analyze the effects of osteocalcin, oleic acid and palmitic acid on CD36. (**A**) Binding mode of CD36 and osteocalcin complexes, with a general view on the left and interaction details on the right. The CD36 protein is shown in blue, and osteocalcin is shown in wheat. The yellow dashed lines indicate hydrogen bond interactions, and the burgundy dashed lines indicate salt bridge interactions. Binding patterns of oleic acid (**B**) and palmitic acid (**C**) to CD36. The left figure shows the total view, and the right figure shows the partial view. The orange bar is the small molecule, and the light blue cartoon is the protein. The blue line indicates hydrogen bonding, the gray dashed line indicates hydrophobicity and the yellow dashed line indicates salt bridge interactions. (**D**) Spatial distribution of osteocalcin, oleic acid and palmitic acid bound to the cell membrane of CD36

Table 2 Interaction types of osteocalcin and CD36

CHAIN A	Residue	CHAIN B	Residue	Interaction type
Osteocalcin	Tyr-87	CD36	Asn-31	Hbond
Osteocalcin	Arg-89	CD36	Tyr-291	Hbond
Osteocalcin	Arg-89	CD36	Glu-282	Hbond
Osteocalcin	Arg-89	CD36	Glu-282	Salt bridge

Table 4 CD36 predicted binding affinity for osteocalcin, oleic acid and palmitic acid

System	Predicted binding affinity (kcal/mol)
CD36-Osteocalcin	-11.0
CD36-Oleic Acid	-6.6
CD36-Palmitic Acid	-5.7

csOCN inhibited the increase in body weight and liver injury in HFD-induced NAFLD mice

We used a HFD to generate NAFLD mice. After C57BL/6J mice were fed a HFD for 11 weeks, the mice were randomized into three groups for a 4-week intervention. The HFD group (HFD group, $n=5$) continued to receive the HFD along with PBS, the low-dose csOCN treatment group (OC-L group, $n=5$) received the HFD and 3 ng/g body weight of the drug, the high-dose csOCN treatment group (OC-H group, $n=5$) received the HFD and 10 ng/g body weight of the drug, and the normal control diet group (NCD group, $n=5$) received a normal diet for 15 weeks (Fig. 9A). As shown in Fig. 9B, we recorded the weekly body weight changes of the mice fed a HFD. Figure 9C shows anatomical drawings and liver images of the mice. These figures shows that the livers of the HFD group became yellow in color, less pliable, and had a granular surface compared to the NCD group. csOCN treatment alleviated these effects. As shown in Fig. 9D-F, the body weight, liver weight, and body weight/liver weight ratio of the mice increased after high-fat induction compared to the mice in the NCD group, and these changes were alleviated after treatment with csOCN. As shown in Fig. 9G-H, the serum ALT and AST levels were significantly increased in NAFLD mice and decreased after csOCN treatment. These findings suggest that csOCN may be used to treat NAFLD mice with weight gain and liver injury.

csOCN inhibits the increase in serum and liver fat in HFD-induced NAFLD mice

To evaluate the effects of csOCN on hepatic steatosis, histopathological examination was performed. We analyzed the livers of each group using H&E and Oil Red O staining. As shown in Fig. 10A-B, the HFD group showed ballooning and obvious lipid droplet staining compared to the NCD group. The ballooning was diminished when the dose of csOCN treatment (in the OC-L and OC-H groups), and lipid droplet staining became weaker. We then examined random blood sugar, blood lipid and liver lipid levels (TG, TC, LDL-C) of the mice separately. The results showed remarkable elevations in the TC, TG and LDL-C levels in the livers of NAFLD mice. Significantly reduced levels of total cholesterol, total cholesterol, and LDL cholesterol were detected after high-dose csOCN treatment (Fig. 10C-E). As shown in Fig. 10F, random blood glucose was elevated in the HFD group compared to the NCD group and decreased after csOCN treatment. As shown in Fig. 10G-I, serum lipid levels were elevated in the HFD group compared to the NCD group and significantly reduced in the high-dose csOCN group. These findings suggested that csOCN ameliorated HFD-induced NAFLD.

In vivo csOCN activates the AMPK-FOXO1/BCL6-CD36 pathway

To further validate the mechanism of action of csOCN in alleviating NAFLD at the animal level, the lipid metabolism-related proteins AMPK, FOXO1, BCL6 and CD36 were detected in the livers of the mice. As shown in Fig. 11, the expression of p-AMPK, FOXO1 and BCL6was lower in HFD-induced NAFLD mice compared to control mice, and CD36 expression was higher. In contrast, csOCN treatment increased the expression of p-AMPK, FOXO1, and BCL6 and decreased the expression of CD36. These findings suggested that csOCN alleviated NAFLD by activating the AMPK pathway.

Discussion

This study shows for the first time that csOCN inhibits CD36 expression and binds to CD36 to inhibit its function. csOCN alleviated lipid accumulation in hepatocytes by reducing CD36 transcription via activation of the AMPK signaling pathway and possible blockade of fatty acid uptake via binding to CD36 on the surface of the cell membrane, which blocks its binding to fatty

Table 3 Interaction types of oleic acid and palmitic acid with CD36

Compound	Protein	Residue	Interaction type
Oleic Acid	CD36	Asn-118	Hbond
Oleic Acid	CD36	Arg-63, Arg-96	Salt bridge
Oleic Acid	CD36	Ala-251, Phe-266, Ile-271, Ile-275, Leu-295, Leu-371, Lys-385, Leu-387	Hydrophobic interaction
Palmitic Acid	CD36	Gly-199	Hbond
Palmitic Acid	CD36	Lys-337	Salt bridge
Palmitic Acid	CD36	Leu-140, Ala-144, Val-198, Val-200, Lys-334, Lys-337, Val-339, Val-389	Hydrophobic interaction

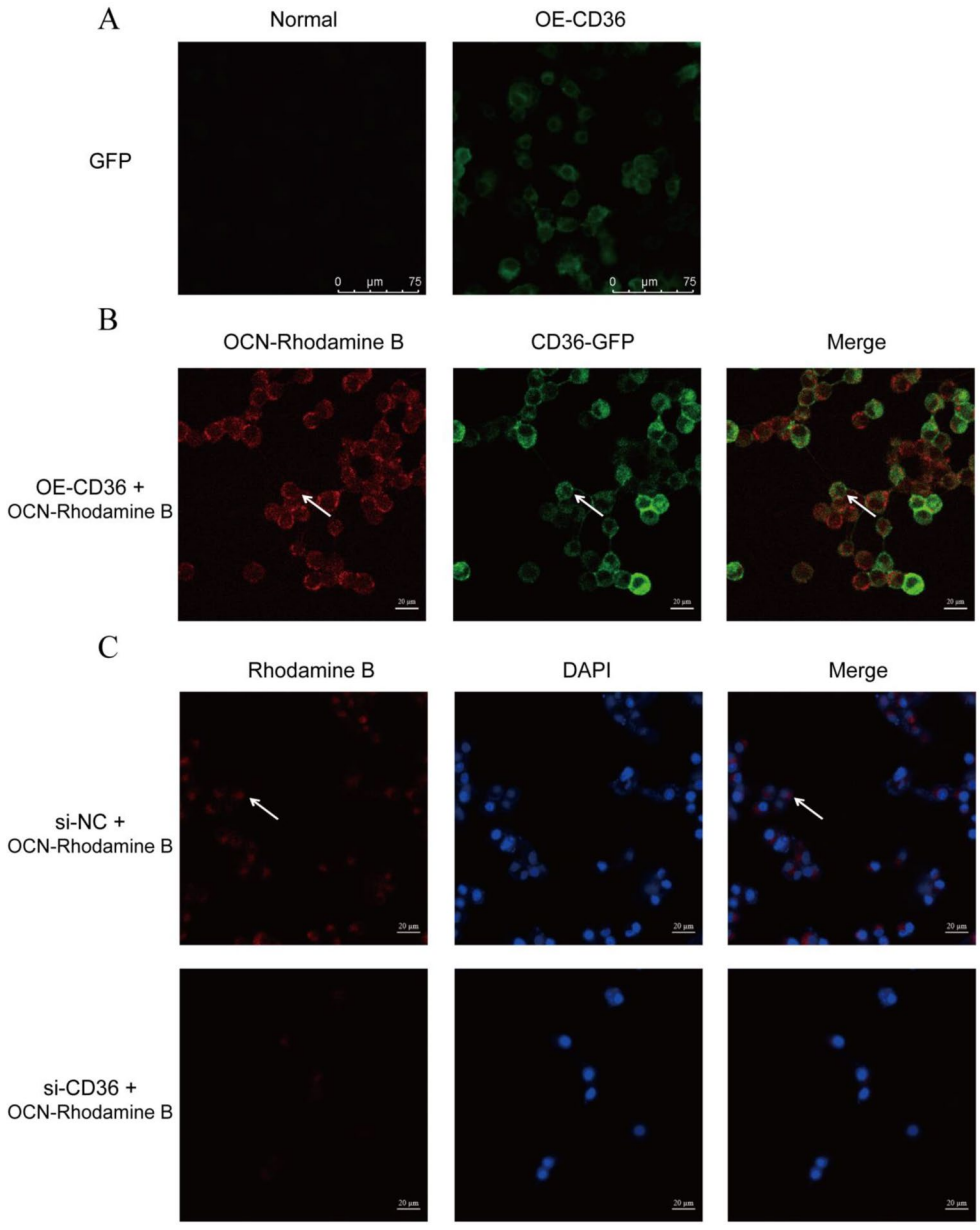

Fig. 8 The colocalization of osteocalcin and CD36. (**A**) GFP fluorescence intensity after lentiviral infection. (**B**) Spatial relationships of lentivirus-infected NCTC 1469 cells treated with rhodamine B-labeled osteocalcin under laser confocal microscopy. (**C**) Spatial relationships of CD36-knockdown NCTC 1469 cells treated with rhodamine B-labeled osteocalcin under laser confocal microscopy. The data are presented as the means ± SD of three independent experiments

acids (Fig. 12). csOCN activated AMPK (Thr172), which increased the FOXO1 expression and and nuclear accumulation, which decreased CD36 transcription. Moreover, activated AMPK promoted the expression of BCL6, which inhibited CD36 transcription.

NAFLD is a metabolic disorder that encompasses a spectrum of changes from hepatocellular steatosis to hepatocellular carcinoma. Abnormalities in the lipid metabolism of hepatocytes lead to hepatocellular steatosis. An increase in the source of fatty acids in hepatocytes or a decrease in consumption leads to an abnormal accumulation of fatty acids in hepatocytes. However, fatty acid uptake plays a major role in NAFLD. CD36, FATPs and FABPs play important roles in fatty acid uptake. OCN plays an important role in energy metabolism. Our previous studies [3, 14] showed that GluOC alleviated lipid accumulation in hepatocytes. The present study first compared the ability of GluOC obtained by prokaryotic expression and chemically synthesized osteocalcin to alleviate hepatocyte lipid accumulation. The results showed that GluOC and csOCN alleviated OA/PA-induced lipid accumulation in hepatocytes. In

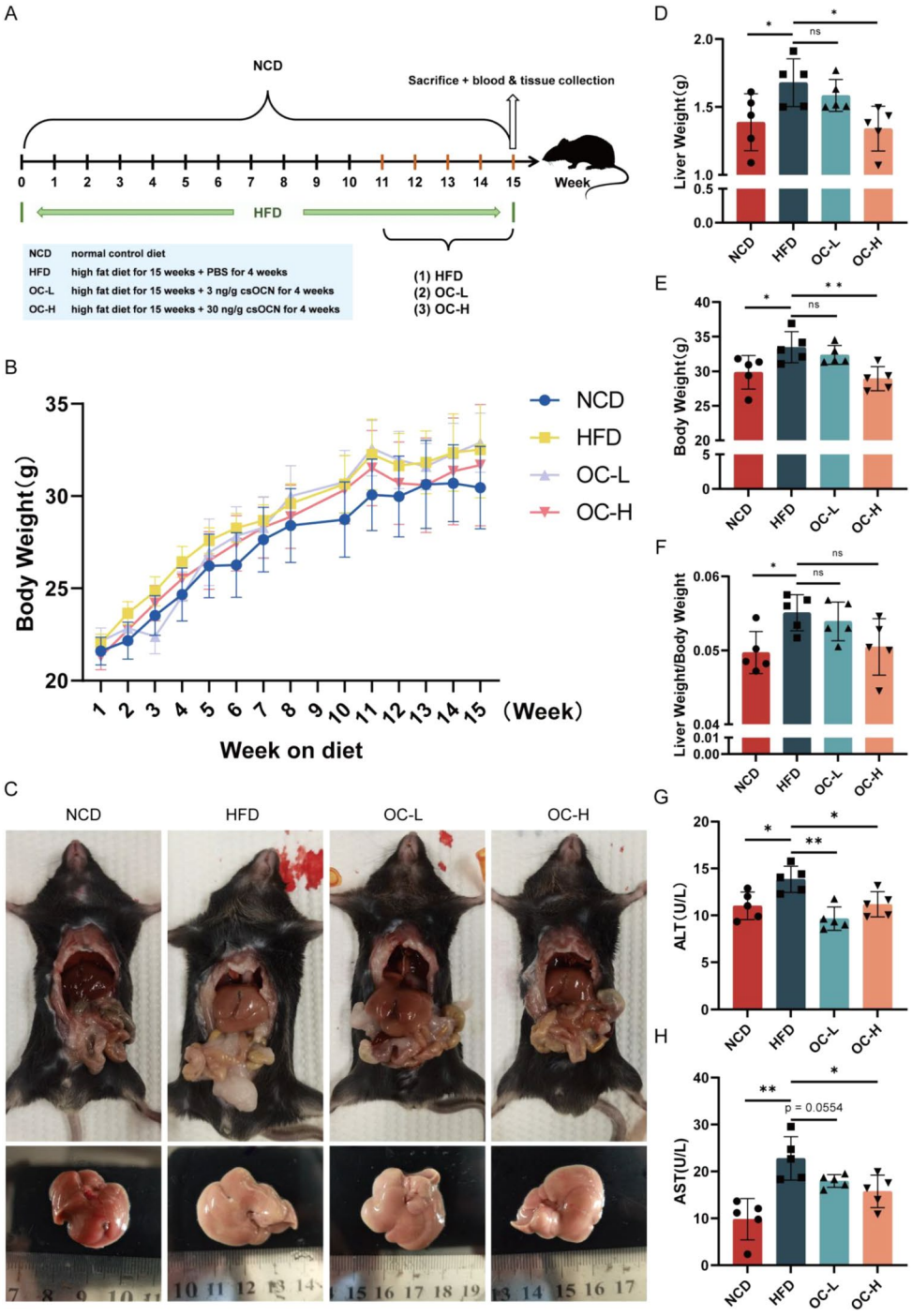

Fig. 9 csOCN inhibited the increase in body weight and liver injury in HFD-induced NAFLD mice. (**A**) Outline of the animal experimental protocols. (**B**) Weekly body weight changes in the mice. (**C**) Anatomical drawings and liver images of the mice. (**D**) Liver weight. (**E**) Body weight. (**F**) Liver/body weight ratio. (**G**) Serum ALT levels. (**H**) Serum AST levels. The data are presented as the means ± SD of five independent experiments. * $p < 0.05$, ** $p < 0.01$

addition, we found that csOCN inhibited the expression of fatty acid uptake-related genes and proteins, particularly CD36. CD36 is a heavily glycosylated 88-kDa class B scavenger receptor that is widely expressed in mammalian cells [15]. CD36 plays a key role in many different types of cancer [16], and it is strongly associated with the development of NAFLD [17]. In adipocytes, dynamic palmitoylation of cell membrane-localized CD36 promotes fatty acid uptake [18]. In the liver, the upregulation of CD36 membrane proteins increases cellular fatty acid uptake and is positively correlated with hepatic steatosis [19–21]. In the present study, CD36 expression was

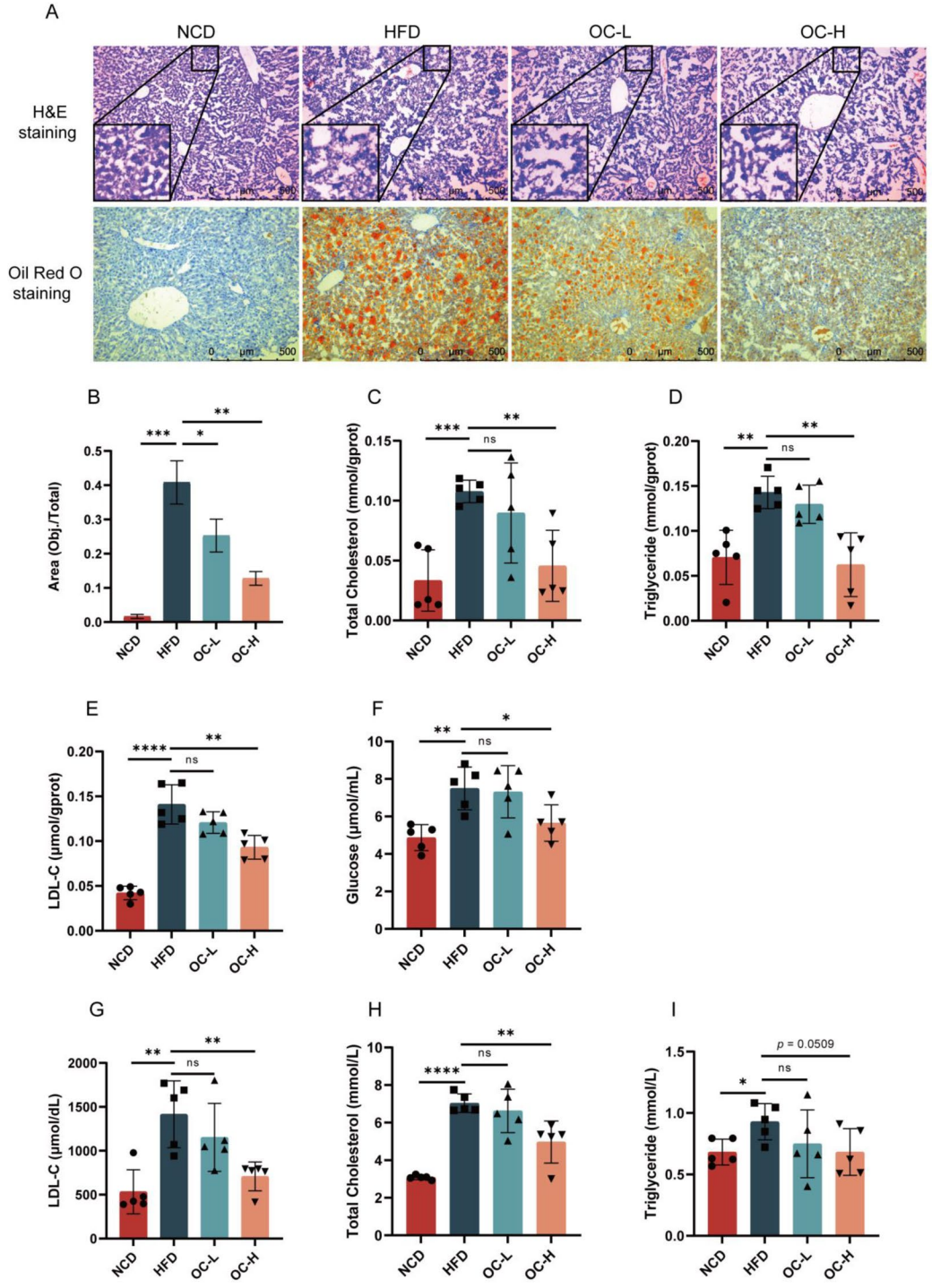

Fig. 10 csOCN inhibited the increase in serum and liver fat in HFD-induced NAFLD mice. (**A**) Results of H&E and Oil Red O staining (100×). (**B**) Quantitative analysis of the Oil Red O staining results in Fig. 10A. Liver lipid content, including total cholesterol (**C**), triglycerides (**D**) and LDL cholesterol (**E**). (**F**) Random blood sugar. Blood lipid content, including serum LDL cholesterol (**G**), serum total cholesterol (**H**) and serum triglycerides (**I**), of mice at week 15. The data are presented as the means ± SD of five independent experiments. * $p < 0.05$, ** $p < 0.01$, *** $p < 0.001$, **** $p < 0.0001$

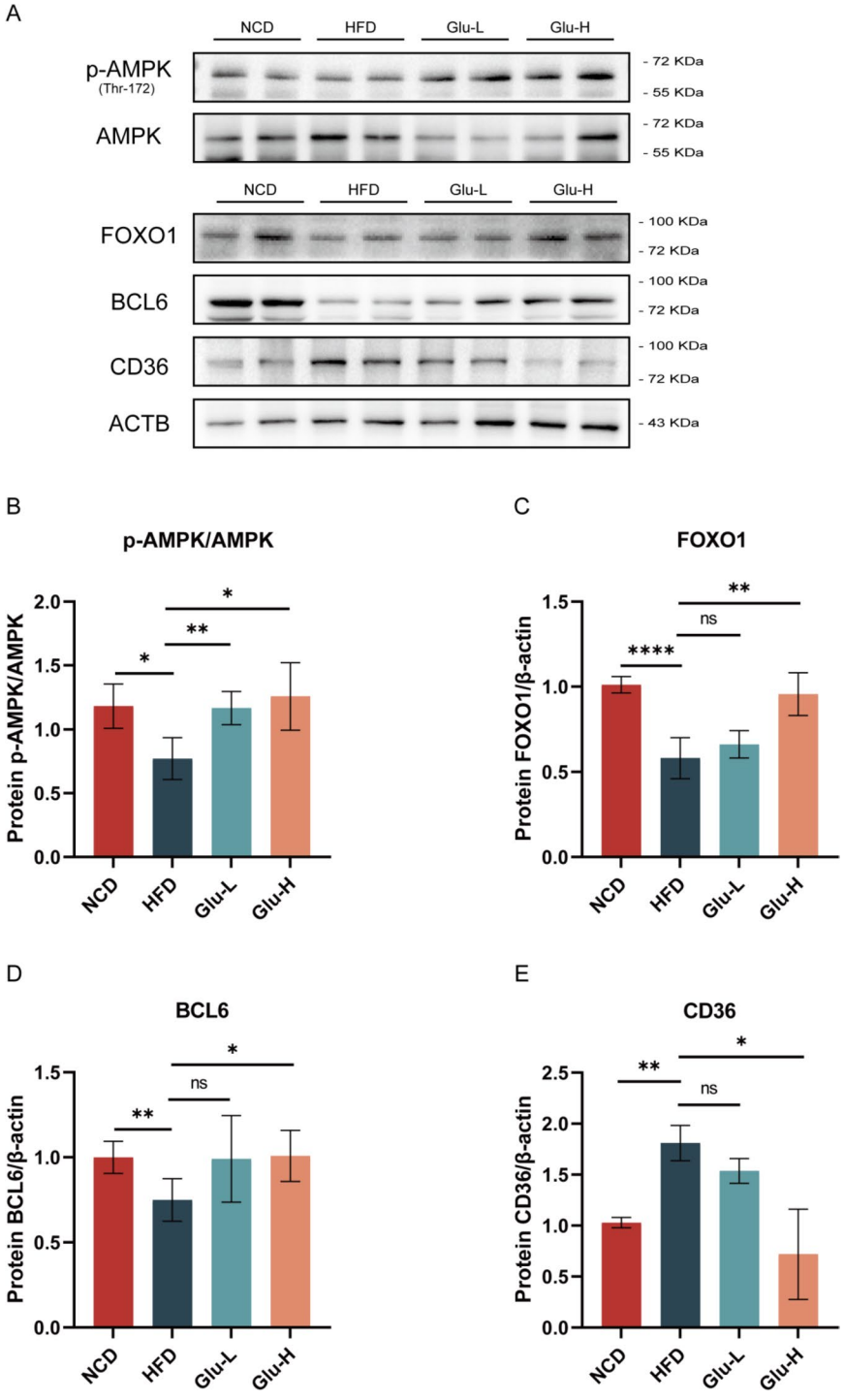

Fig. 11 csOCN activates the AMPK signaling pathway. (**A**) Effects of a HFD and csOCN treatment on relevant proteins in the AMPK pathway and quantitative analysis of p-AMPK (**B**), FOXO1 (**C**), BCL6 (**D**) and CD36 (**E**). The data are presented as the means ± SD of three independent experiments. * $p < 0.05$, ** $p < 0.01$, *** $p < 0.001$

increased in hepatocytes induced by a HFD or OA/PA, and fatty acid uptake was increased. In contrast, csOCN treatment inhibited the CD36 expression and fatty acid uptake pathways. CD36 may mediate the role of csOCN in alleviating NAFLD.

AMPK is a kinase that regulates lipid metabolism, and it is a potential therapeutic target for metabolic diseases. AMPK plays an important role in fatty acid oxidation [22] and the inhibition of inflammation and oxidative stress [6]. Our previous results showed that GluOC activated

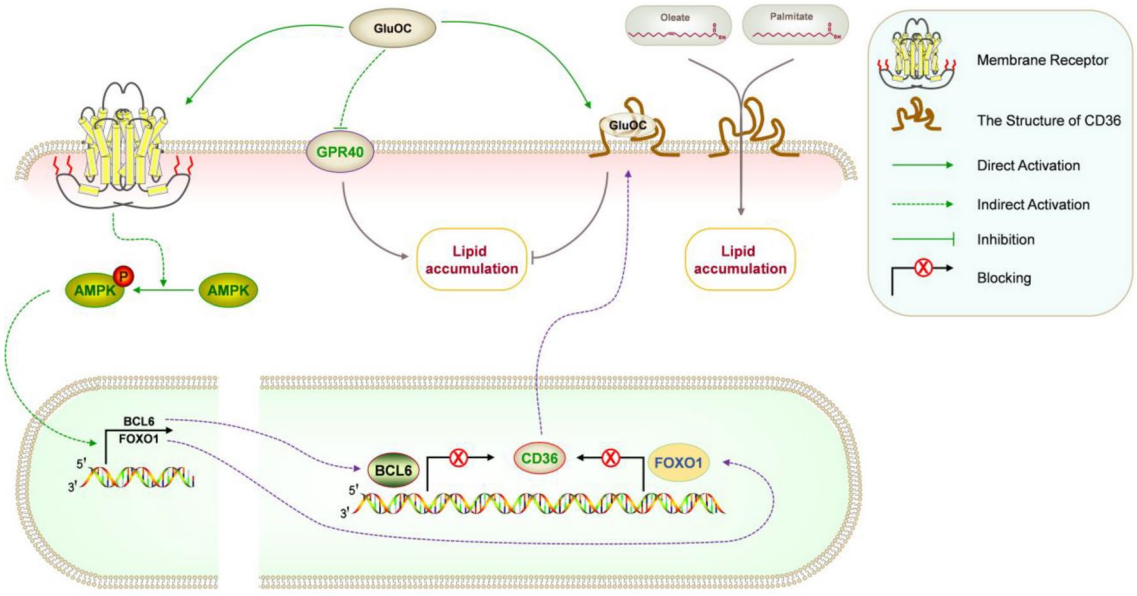

Fig. 12 Working hypothesis of the effects of csOCN

AMPK via the cell membrane receptor GPRC6A, downregulated SREBP-1c and SCD1, and blocked the de novo synthesis of fatty acids [3]. CpdC (an AMPK inhibitor) did not alter the overall domain organization or complex conformation of the inhibited AMPK [23]. In the present study, OA/PA inhibited AMPK phosphorylation, and csOCN promoted AMPK phosphorylation and inhibited CD36 expression. CpdC was used to block the inhibition of AMPK phosphorylation, and the inhibitory effect of csOCN on CD36 was attenuated. These findings suggest that AMPK mediates csOCN regulation of CD36.

FOXO1 (Forkhead box protein O1) primarily consists of an N-terminal structural domain (NTD), a DNA-binding forkhead structural domain (FDH), a nuclear localization (NLS) region, a nuclear export (NES) region and a C-terminal transcriptional activation domain (TAD), and it plays a crucial role in mammalian life. After nuclear translocation of FOXO1, FDH binds to DNA to inhibit or activate the gene expression of target proteins [24, 25]. FOXO1 binds to the CD36 promoter region to suppress CD36 transcription [26, 27]. Activated AMPK (Thr-172) was found to increase FOXO1 expression [28]. These results are consistent with our findings. In our study, csOCN promoted FOXO1 expression, and the effect of csOCN was reversed by the addition of CpdC. Meanwhile, laser confocal microscopy results revealed enhanced nuclear localization of FOXO1 after csOCN treatment compared to the OA/PA group, and CpdC reversed this increase. These results suggest that activation of AMPK by csOCN increases FOXO1 expression, its nuclear accumulation and ultimately leads to the inhibition of CD36 expression.

Moreover, BCL6 (B-cell lymphoma 6) is a transcriptional suppressor and proto-oncogene that is a master regulator of humoral immunity and lymphoma survival [29, 30]. In addition to affecting cancer, it plays an important role in energy metabolism. For example, one study revealed a role for BCL6 in suppressing genes that are important for glycolysis and related pathways [31]. The 79−6 (a BCL6 inhibitor) selectively inhibits the transcriptional suppression activity of BCL6 without affecting BCL6 protein levels. We found that csOCN promoted AMPK activation by increasing BCL6 expression and decreasing CD36 expression. However, the addition of 79−6 reversed the ability of csOCN to inhibit CD36 expression. Previous results showed that BCL6 alleviated NAFLD in mice via suppression of the fatty acid transporter CD36 [32]. These results suggest that csOCN alleviates lipid accumulation in hepatocytes via the AMPK-BCL6-CD36 pathway.

Additionally, NAFLD mice were generated using a previously established experimental method [33] and subsequently treated with csOCN. The results showed that high concentrations of csOCN decreased the levels of serum and liver TG, TC, and LDL-C compared to the NAFLD group. The levels of phosphorylated AMPK, FOXO1 and BCL6 were increased after csOCN treatment, and the expression of CD36 was decreased, according to the subsequent analysis of AMPK pathway-related proteins. In conclusion, csOCN alleviated NAFLD via the AMPK-FOXO1/BCL6-CD36 pathway.

The structure of a protein determines its function, and we analyzed the structure of CD36 on the cell membrane and its effect on fatty acid uptake. We summarized the structure of CD36 based on an extensive literature search

(Fig. 7D) [16, 34–37]. The structural basis for CD36 binding to FAs is based on two very short intracytoplasmic domains and a large, highly glycosylated extracellular domain [38]. A large hydrophobic pocket (binding pocket 1) at the proximal N-terminus of CD36 outside the cell membrane is the main ligand transport tunnel [39], but another hydrophobic pocket (binding pocket 2) at the proximal C-terminus may be the main channel for fatty acid transport [40]. Molecular docking via computer simulation confirmed the presence of binding sites for CD36 with osteocalcin, oleic acid and palmitic acid. We found that when osteocalcin bound to CD36, it covered the two hydrophobic pockets of CD36, and oleic acid and palmitic acid also covered these two hydrophobic pockets. Because OCN, oleic acid, and palmitic acid overlapped in the spatial distribution of CD36, and OCN bound to CD36 more strongly than oleic acid or palmitic acid (Table 4), OCN binding to CD36 may block the bingding of oleic acid and palmitic acid (Fig. 7D). Similarly, a previous study reported [41] that NAFLD01 may be used as a CD36-specific aptamer for the treatment of NAFLD because NAFLD01 is highly likely to bind the CD36 amino acid sequence 30–439, which is also an extracellular amino acid residue of CD36. We found that osteocalcin colocalized with CD36 using laser confocal microscopy, and our results suggest that osteocalcin may binds directly to CD36 to influence the binding of fatty acids to CD36.

Conclusions

In this study, we investigated the mechanism by which csOCN alleviates NAFLD using an NAFLD animal model and an NAFLD cell model. csOCN inhibited the expression of CD36 after activation of the AMPK signaling pathway, which alleviated hepatocyte steatosis. The results of the present study showed that activation of AMPK by csOCN promoted FOXO1 expression and nuclear localization and increasing BCL6 expression, which in turn inhibited CD36 expression and alleviated lipid accumulation in hepatocytes. We also proposed for the first time that osteocalcin may interact directly with CD36. Molecular docking results showed that osteocalcin, oleic acid, and palmitic acid bound to CD36, and osteocalcin had the strongest binding to CD36. We also confirmed that osteocalcin can colocalized with CD36. These findings suggest that osteocalcin may bind to CD36 and blocks fatty acid uptake by CD36. This study provides new ideas for the prevention and control of NAFLD.

Acknowledgements
We appreciate to the School of Life Sciences, University of Chinese Academy of Sciences for providing experimental instruments and technical supports.

Author contributions
Conceptualization, M.Z. and J.Y.; methodology, M.Z., K.D., and Q.D.; software, M.Z.; validation, M.Z., K. D., Q.D., and J.Y.; formal analysis, M.Z., J.X., X.B., and L.C.; investigation, M.Z.; resources, M.Z.; data curation, M.Z.; writing—original draft preparation, M.Z.; writing—review and editing, M.Z., and J.Y.; visualization, M.Z.; supervision, J.Y.; project administration, J.Y.; funding acquisition, J.Y. All authors have read and agreed to the published version of the manuscript.

Funding
This work was supported by the Fundamental Research Funds for the Central Universities (Grant No. E2E43202X2).

Data availability
The data presented in this study are available on request from the corresponding author.

Declarations

Institutional review board statement
Animal studies were approved by the University of Chinese Academy of Sciences Animal Care and Use Committee (UCAS-A-2022-03-03).

Informed consent
Not applicable.

Sample availability
Samples of the compounds are available from the authors.

Conflict of interest
The authors declare no conflict of interest.

Received: 21 April 2024 / Accepted: 9 August 2024
Published online: 22 August 2024

References

1. Powell EE, Wong VW, andRinella M. (2021) Non-alcoholic fatty liver disease Lancet 397, 2212–24. https://doi.org/10.1016/S0140-6736(20)32511-3
2. Huh Y, Cho YJ, andNam GE. Recent epidemiology and risk factors of nonalcoholic fatty liver disease. J Obes Metab Syndr. 2022;31:17–27. https://doi.org/10.7570/jomes22021.
3. Wang D, Zhang M, Xu J, andYang J. (2023) Uncarboxylated osteocalcin decreases SCD1 by activating AMPK to alleviate hepatocyte lipid Accumulation molecules 28, 3121. https://doi.org/10.3390/molecules28073121
4. Hosseini S, Naderi-Manesh H, Vali H, Baghaban Eslaminejad M, Azam Sayahpour F, Sheibani S, andFaghihi S. Contribution of osteocalcin-mimetic peptide enhances osteogenic activity and extracellular matrix mineralization of human osteoblast-like cells. Colloids Surf B Biointerfaces. 2019;173:662–71. https://doi.org/10.1016/j.colsurfb.2018.10.035.
5. Yan Y, Zhou XE, Xu HE, andMelcher K. Structure and physiological regulation of AMPK. Int J Mol Sci. 2018;19:3534. https://doi.org/10.3390/ijms19113534.
6. Liu Y, Li D, Wang S, Peng Z, Tan Q, He Q, andWang J. 6-Gingerol ameliorates hepatic steatosis, inflammation and oxidative stress in High-Fat Diet-Fed mice through activating LKB1/AMPK signaling. Int J Mol Sci. 2023;24:6285. https://doi.org/10.3390/ijms24076285.
7. Garcia D, Hellberg K, Chaix A, Wallace M, Herzig S, Badur M G, et al. Genetic liver-specific AMPK activation protects against Diet-Induced obesity and NAFLD. Cell Rep. 2019;26:192–208. https://doi.org/10.1016/j.celrep.2018.12.036. e196.
8. Diniz TA, de Lima Junior EA, Teixeira AA, Biondo LA, da Rocha LAF, Valadao IC et al. (2021) Aerobic training improves NAFLD markers and insulin resistance through AMPK-PPAR-alpha signaling in obese mice Life Sci 266, 118868 https://doi.org/10.1016/j.lfs.2020.118868
9. Hao JW, Wang J, Guo H, Zhao YY, Sun HH, Li YF, et al. CD36 facilitates fatty acid uptake by dynamic palmitoylation-regulated endocytosis. Nat Commun. 2020;11:4765. https://doi.org/10.1038/s41467-020-18565-8.
10. Zeng H, Qin H, Liao M, Zheng E, Luo X, Xiao A, et al. CD36 promotes de novo lipogenesis in hepatocytes through INSIG2-dependent SREBP1 processing. Mol Metab. 2022;57:101428. https://doi.org/10.1016/j.molmet.2021.101428.

11. Samovski D, Sun J, Pietka T, Gross RW, Eckel RH, Su X et al. (2015) Regulation of AMPK activation by CD36 links fatty acid uptake to beta-oxidation diabetes 64, 353–9 https://doi.org/10.2337/db14-0582
12. Nassir F, Adewole OL, Brunt EM, andAbumrad NA. CD36 deletion reduces VLDL secretion, modulates liver prostaglandins, and exacerbates hepatic steatosis in ob/ob mice. J Lipid Res. 2013;54:2988–97. https://doi.org/10.1194/jlr.M037812.
13. Li Y, Yang P, Zhao L, Chen Y, Zhang X, Zeng S, et al. CD36 plays a negative role in the regulation of lipophagy in hepatocytes through an AMPK-dependent pathway. J Lipid Res. 2019;60:844–55. https://doi.org/10.1194/jlr.M090969.
14. Zhang XL, Wang YN, Ma LY, Liu ZS, Ye F, andYang JH. Uncarboxylated osteocalcin ameliorates hepatic glucose and lipid metabolism in KKAy mice via activating insulin signaling pathway. Acta Pharmacol Sin. 2020;41:383–93. https://doi.org/10.1038/s41401-019-0311-z.
15. Chen Y, Zhang J, Cui W, andSilverstein RL. CD36, a signaling receptor and fatty acid transporter that regulates immune cell metabolism and fate. J Exp Med. 2022;219:e20211314. https://doi.org/10.1084/jem.20211314.
16. Feng WW, Zuppe HT, andKurokawa M. (2023) The role of CD36 in Cancer Progression and its value as a therapeutic target cells 12, 1605 https://doi.org/10.3390/cells12121605
17. Rada P, Gonzalez-Rodriguez A, Garcia-Monzon C, andValverde AM. Understanding lipotoxicity in NAFLD pathogenesis: is CD36 a key driver? Cell Death Dis. 2020;11:802. https://doi.org/10.1038/s41419-020-03003-w.
18. Wang J, Hao JW, Wang X, Guo H, Sun HH, Lai XY, et al. DHHC4 and DHHC5 facilitate fatty acid uptake by palmitoylating and targeting CD36 to the plasma membrane. Cell Rep. 2019;26(209–221 e205). https://doi.org/10.1016/j.celrep.2018.12.022.
19. Yang Z, Huang X, Zhang J, You K, Xiong Y, Fang J, et al. Hepatic DKK1-driven steatosis is CD36 dependent. Life Sci Alliance. 2023;6:e202201665. https://doi.org/10.26508/lsa.202201665.
20. Miquilena-Colina ME, Lima-Cabello E, Sanchez-Campos S, Garcia-Mediavilla MV, Fernandez-Bermejo M, Lozano-Rodriguez T, et al. Hepatic fatty acid translocase CD36 upregulation is associated with insulin resistance, hyperinsulinaemia and increased steatosis in non-alcoholic steatohepatitis and chronic hepatitis C. Gut. 2011;60:1394–402. https://doi.org/10.1136/gut.2010.222844.
21. Koonen DP, Jacobs RL, Febbraio M, Young ME, Soltys CL, Ong H et al. (2007) Increased hepatic CD36 expression contributes to dyslipidemia associated with diet-induced obesity diabetes 56, 2863–71 https://doi.org/10.2337/db07-0907
22. Park SH, Gammon SR, Knippers JD, Paulsen SR, Rubink DS, andWinder WW. Phosphorylation-activity relationships of AMPK and acetyl-CoA carboxylase in muscle. J Appl Physiol (1985). 2002;92:2475–82. https://doi.org/10.1152/japplphysiol.00071.2002.
23. Yan Y, Mukherjee S, Harikumar KG, Strutzenberg TS, Zhou XE, Suino-Powell K, et al. Structure of an AMPK complex in an inactive. ATP-bound State Sci. 2021;373:413–9. https://doi.org/10.1126/science.abe7565.
24. Evans-Anderson HJ, Alfieri CM, andYutzey KE. Regulation of cardiomyocyte proliferation and myocardial growth during development by FOXO transcription factors. Circ Res. 2008;102:686–94. https://doi.org/10.1161/CIRCRESAHA.107.163428.
25. Huang H, andTindall DJ. Dynamic FoxO transcription factors. J Cell Sci. 2007;120:2479–87. https://doi.org/10.1242/jcs.001222.
26. Ren B, Best B, Ramakrishnan DP, Walcott BP, Storz P, andSilverstein RL. LPA/PKD-1-FoxO1 signaling Axis mediates endothelial cell CD36 transcriptional repression and proangiogenic and proarteriogenic reprogramming arterioscler. Thromb Vasc Biol. 2016;36:1197–208. https://doi.org/10.1161/ATVBAHA.116.307421.
27. Song Y, Zhang J, Jiang C, Song X, Wu H, Zhang J, et al. FOXO1 regulates the formation of bovine fat by targeting CD36 and STEAP4. Int J Biol Macromol. 2023;248:126025. https://doi.org/10.1016/j.ijbiomac.2023.126025.
28. Awad H, Nolette N, Hinton M, andDakshinamurti S. (2014) AMPK and FoxO1 regulate catalase expression in hypoxic pulmonary arterial smooth muscle Pediatr Pulmonol 49, 885–97 https://doi.org/10.1002/ppul.22919
29. Cardenas MG, Oswald E, Yu W, Xue F, MacKerell AD Jr., andMelnick AM. The expanding role of the BCL6 oncoprotein as a Cancer Therapeutic Target. Clin Cancer Res. 2017;23:885–93. https://doi.org/10.1158/1078-0432.CCR-16-2071.
30. Louwen F, Kreis NN, Ritter A, Friemel A, Solbach C, andYuan J. BCL6, a key oncogene, in the placenta. pre-eclampsia Endometr Hum Reprod Update. 2022;28:890–909. https://doi.org/10.1093/humupd/dmac027.
31. Oestreich KJ, Read KA, Gilbertson SE, Hough KP, McDonald PW, Krishnamoorthy V, andWeinmann AS. Bcl-6 directly represses the gene program of the glycolysis pathway. Nat Immunol. 2014;15:957–64. https://doi.org/10.1038/ni.2985.
32. Zhang H, Li Y, Zhang C, Huang K, Zhao J, Le S, et al. B-cell lymphoma 6 alleviates nonalcoholic fatty liver disease in mice through suppression of fatty acid transporter CD36. Cell Death Dis. 2022;13. https://doi.org/10.1038/s41419-022-04812-x.
33. Zhang M, Bai X, Du Q, Xu J, Wang D, Chen L, et al. The different mechanisms of lipid Accumulation in Hepatocytes Induced by Oleic Acid/Palmitic Acid and High-Fat Diet. Molecules. 2023;28:6714. https://doi.org/10.3390/molecules28186714.
34. Kuda O, Pietka TA, Demianova Z, Kudova E, Cvacka J, Kopecky J, andAbumrad NA. Sulfo-N-succinimidyl oleate (SSO) inhibits fatty acid uptake and signaling for intracellular calcium via binding CD36 lysine 164: SSO also inhibits oxidized low density lipoprotein uptake by macrophages. J Biol Chem. 2013;288:15547–55. https://doi.org/10.1074/jbc.M113.473298.
35. Shu H, Peng Y, Hang W, Nie J, Zhou N, andWang DW. The role of CD36 in cardiovascular disease. Cardiovasc Res. 2022;118:115–29. https://doi.org/10.1093/cvr/cvaa319.
36. Pepino MY, Kuda O, Samovski D, andAbumrad NA. Structure-function of CD36 and importance of fatty acid signal transduction in fat metabolism. Annu Rev Nutr. 2014;34:281–303. https://doi.org/10.1146/annurev-nutr-071812-161220.
37. Yang X, Okamura DM, Lu X, Chen Y, Moorhead J, Varghese Z, andRuan XZ. CD36 in chronic kidney disease: novel insights and therapeutic opportunities. Nat Rev Nephrol. 2017;13:769–81. https://doi.org/10.1038/nrneph.2017.126.
38. Li Y, Huang X, Yang G, Xu K, Yin Y, Brecchia G, andYin J. CD36 favours fat sensing and transport to govern lipid metabolism. Prog Lipid Res. 2022;88:101193. https://doi.org/10.1016/j.plipres.2022.101193.
39. Park YM. CD36, a scavenger receptor implicated in atherosclerosis. Exp Mol Med. 2014;46:e99. https://doi.org/10.1038/emm.2014.38.
40. Zhang X, Fan J, Li H, Chen C, andWang Y. (2021) CD36 signaling in Diabetic Cardiomyopathy Aging Dis 12, 826–40 https://doi.org/10.14336/AD.2020.1217
41. Pu Y, Xiang J, Zhang X, Deng Y, Liu H, andTan W. CD36 as a molecular target of functional DNA aptamer NAFLD01 selected against NAFLD. Cells Anal Chem. 2021;93:3951–8. https://doi.org/10.1021/acs.analchem.0c04866.

Publisher's Note